Determining Nanocapillary Geometry from Electrochemical Impedance Spectroscopy Using a Variable Topology Network Circuit Model

ARTICLE *in* ANALYTICAL CHEMISTRY · JANUARY 2011

Impact Factor: 5.64 · DOI: 10.1021/ac102236k · Source: PubMed

3 AUTHORS, INCLUDING:

Shaurya Prakash

The Ohio State University

52 PUBLICATIONS **412** CITATIONS

SEE PROFILE

Anal. Chem. **2011,** *83,* 533–541

Determining Nanocapillary Geometry from Electrochemical Impedance Spectroscopy Using a Variable Topology Network Circuit Model

Michael J. Vitarelli, Jr.,[†] Shaurya Prakash,*[,‡] and David S. Talaga*[,§]

Department of Chemistry and Chemical Biology, Rutgers University, 610 Taylor Road, Piscataway, New Jersey 08854, United States, Department of Mechanical Engineering, The Ohio State University, 201 West 19th Avenue, Columbus, Ohio 43210, United States, and Department of Chemistry and Biochemistry, Montclair State University, 1 Normal Road, Montclair, New Jersey 07043, United States

Solid-state nanopores and nanocapillaries find increasing use in a variety of applications including DNA sequencing, synthetic nanopores, next-generation membranes for water purification, and other nanofluidic structures. This paper develops the use of electrochemical impedance spectroscopy to determine the geometry of nanocapillaries. A network equivalent circuit element is derived to include the effects of the capacitive double layer inside the nanocapillaries as well as the influence of varying nanocapillary radius. This variable topology function is similar to the finite Warburg impedance in certain limits. Analytical expressions for several different nanocapillary shapes are derived. The functions are evaluated to determine how the impedance signals will change with different nanocapillary aspect ratios and different degrees of constriction or inflation at the capillary center. Next, the complex impedance spectrum of a nanocapillary array membrane is measured at varying concentrations of electrolyte to separate the effects of nanocapillary double layer capacitance from those of nanocapillary geometry. The variable topology equivalent circuit element model of the nanocapillary is used in an equivalent circuit model that included contributions from the membrane and the measurement apparatus. The resulting values are consistent with the manufacturer's specified tolerances of the nanocapillary geometry. It is demonstrated that electrochemical impedance spectroscopy can be used as a tool for in situ determination of the geometry of nanocapillaries.

Individual solid-state nanopores or nanocapillary array membranes (NCAMs) are routinely fabricated[1,2] and have been used extensively in recent years to develop synthetic systems for ion-channel studies,[3−7] single molecule sensing,[8,9] DNA sequencing,[1,10] nanofabrication templates,[11,12] and fundamental studies of ionic flow at the nanoscale.[13,14] Track-etched arrays of nanocapillaries in polymeric membranes[15,16] are commercially available and have been used for permselectivity,[17] as molecular gates for nanoscale flow control,[18] and for identification of transport regimes as a function of electrokinetic radius.[14] These applications established that solution-phase transport through the membrane is affected by the geometry and surface properties of the nanocapillaries both of which can change depending on solution conditions.[19,20] Therefore, in situ methods for determining the geometry and surface properties of nanocapillaries are vital for understanding analyte transport and analyte−capillary interactions.

Ideally, in situ characterization of the nanocapillary geometry would be by a nondestructive method that is based on the transport physics relevant to the intended application. High-

* To whom correspondence should be addressed. E-mail: prakash.31@osu.edu (S.P.); talaga@rutgers.edu (D.S.T.).

[†] Rutgers University.

[‡] The Ohio State University.

[§] Montclair State University.

(1) Dekker, C. *Nat. Nanotechnol.* **2007**, *2*, 209–215.

(2) Piruska, A.; Gong, M.; Sweedler, J. V.; Bohn, P. W. *Chem. Soc. Rev.* **2010**, *39*, 1060–1072.

(3) Tian, Y.; Hou, X.; Wen, L.; Guo, W.; Song, Y.; Sun, H.; Wang, Y.; Jiang, L.; Zhu, D. *Chem. Commun.* **2010**, *46*, 1682–1682.

(4) Siwy, Z.; Howorka, S. *Chem. Soc. Rev.* **2010**, *39*, 1115–1132.

(5) Holt, J. K.; Park, H. G.; Wang, Y.; Stadermann, M.; Artyukhin, A. B.; Grigoropoulos, C. P.; Noy, A.; Bakajin, O. *Science* **2006**, *312*, 1034–1037.

(6) Siwy, Z.; Heins, E.; Harrell, C.; Kohli, P.; Martin, C. *J. Am. Chem. Soc.* **2004**, *126*, 10850–10851.

(7) Steinle, E.; Mitchell, D.; Wirtz, M.; Lee, S.; Young, V. Y.; Martin, C. *Anal. Chem.* **2002**, *74*, 2416–2422.

(8) Howorka, S.; Siwy, Z. *Chem. Soc. Rev.* **2009**, *38*, 2360–2384.

(9) Chen, Z.; Jiang, Y.; Dunphy, D. R.; Adams, D. P.; Hodges, C.; Liu, N.; Zhang, N.; Xomeritakis, G.; Jin, X.; Aluru, N. R.; Gaik, S. J.; Hillhouse, H. W.; Brinker, C. J. *Nat. Mater.* **2010**, *9*, 667–675.

(10) Branton, D.; Marziali, A.; Deamer, D. W.; Bayley, H.; Benner, S. A.; Butler, T.; Di Ventra, M.; Garaj, S.; Hibbs, A.; Huang, X.; Jovanovich, S. B.; Krstic, P. S.; Lindsay, S.; Ling, X. S.; Mastrangelo, C. H.; Meller, A.; Oliver, J. S.; Pershin, Y. V.; Ramsey, J. M.; Riehn, R.; Soni, G. V.; Tabard-Cossa, V.; Wanunu, M.; Wiggin, M.; Schloss, J. A. *Nat. Biotechnol.* **2008**, *26*, 1146–1153.

(11) Gultepe, E.; Nagesha, D.; Menon, L.; Busnaina, A.; Sridhar, S. *Appl. Phys. Lett.* **2007**, *90*, 163119/1–163119/3.

(12) Lu, Z.; Namboodiri, A.; Collinson, M. *ACS Nano* **2008**, *2*, 993–999.

(13) Raghunathan, A. V.; Aluru, N. R. *Phys. Rev. E: Stat., Nonlinear, Soft Matter Phys.* **2007**, *76*, 011202/1–011202/12.

(14) Kemery, P. J.; Steehler, J. K.; Bohn, P. W. *Langmuir* **1998**, *14*, 2884–2889.

(15) Lee, S. B.; Martin, C. R. *J. Am. Chem. Soc.* **2002**, *124*, 11850–11851.

(16) Prakash, S.; Yeom, J.; Jin, N.; Adesida, I.; Shannon, M. A. *Proc. Inst. Mech. Eng., Part N* **2007**, *220*, 45–52.

(17) Nishizawa, M.; Menon, V. P.; Martin, C. R. *Science* **1995**, *268*, 700–702.

(18) Tulock, J. J.; Shannon, M. A.; Bohn, P. W.; Sweedler, J. V. *Anal. Chem.* **2004**, *76*, 6419–6425.

(19) Prakash, S.; Karacor, M. B.; Banerjee, S. *Surf. Sci. Rep.* **2009**, *64*, 233–254.

(20) Prakash, S.; Piruska, A.; Gatimu, E. N.; Bohn, P. W.; Sweedler, J. V.; Shannon, M. A. *IEEE Sens. J.* **2008**, *8*, 441–450.

10.1021/ac102236k
Published on Web 12/28/2010

resolution electron microscopy can image the geometry;[21−23] however, it requires extensive sample preparation, usually rendering the sample unusable for its application. Current−voltage measurements have been reported that show evidence of surface-charge related rectification.[24−26] These dc-based methods do not give direct information about the geometry of the nanocapillaries. By contrast, electrochemical impedance spectroscopy, or EIS,[27−29] measures the impedance as a function of frequency of applied ac potential.

Since the EIS signal is a measure of the electrokinetic transport of ionic solution through the nanocapillaries, it is sensitive to their geometry and surface electrical properties.[30,31] The measured signal is governed by electrokinetic transport equations that are laborious to implement for characterization of arbitrary nanofluidic systems[32] and therefore are not practical for routine laboratory use. Equivalent circuit modeling is a standard approach to fitting EIS data.[33,34] Nanocapillary physical parameters such as geometry and double layer differential capacitance must be interpreted from the fit parameters. A disadvantage of this approach is multiple equivalent circuits can be fit to the same data. This problem increases as the number of equivalent circuit elements in the model increases. Therefore, the number of elements required in an equivalent circuit model should be minimized while still capturing the relevant physics.

EIS has been previously applied to NCAMs. In these cases $R||C$ circuits have been used to extract resistive and capacitive properties, the effect of a dc bias on these properties, and the effects of foulants on the NCAMs.[16,35−38] However, $R||C$ equivalent circuit models have not been used to quantify the geometry of the nanocapillaries. Moreover, specific equivalent circuit models have not been developed that explicitly include details of the nanocapillary geometry and surface properties.

The purpose of this paper is to develop a new equivalent circuit element that, when coupled with the standard approach of equivalent circuit modeling, can obtain the nanocapillaries geometry and double layer differential capacitance. Previously, a related equivalent circuit model was used to derive expressions to determine the average shape of closed capacitive pores.[39] The new equivalent circuit element predicts that the shape of EIS data will depend on the aspect ratio of the capillaries and on any constrictions present in the capillaries. These geometric effects would be indeterminable from simple current−voltage curves that give the zero-frequency dc limit of the impedance. Formulas for several specific parametrized nanocapillary geometries are derived and compared with experimental data. The new impedance element was used to model EIS measurements on an NCAM of nominal pore radius of 5 nm. Measurements at different solution conductivities were used to separate the effects of geometry and double layer differential capacitance in the EIS data. The new impedance element was able to invert EIS data to nanocapillary geometry when used in a simple equivalent circuit model that also included the response of the membrane and experimental apparatus. The limitations and assumptions of the model are critically discussed in terms of its ability to reproduce the data and nanocapillary parameters.

METHODS

Two glass chambers sandwich two cylindrical pieces of poly(dimethylsiloxane) (PDMS), with a NCAM (GE KN1CP02500) in between. The manufacturer specified that the NCAM has nanocapillary density of 6×10^8 capillaries/cm^2 ± 15%, a thickness of 6 μm ± 10%, prepared by track etching for a nominal pore radius of 5 nm +0% −20%. The glass chambers contain 5 mL of the test electrolyte solution in 18 MΩ Millipore water with a known concentration of electrolytes as discussed below. Ag/AgCl reference electrodes (MF-2052, Bioanalytical Systems, Inc.) and gold wire counter electrodes were used. The PDMS cylinders have a 0.60 cm diameter hole for an exposed NCAM surface area A_{mem} of 0.283 cm^2. The PDMS pieces are bonded following exposure to 30 W oxygen plasma.[40−42] All experiments were performed in a copper mesh Faraday cage to minimize electrical noise. The Au counter electrodes were RCA-1 cleaned before each experiment.[43] A schematic of the experimental setup is located in the Supporting Information.

NCAMs require equilibration prior to use.[7] Prior to use, the membranes were soaked in 18 MΩ Millipore water for 48 h. Prior to each experiment, they were soaked at the experimental solution conditions for 4 h. It is critical to maintain a constant pH so as to preserve the membrane surface charge density,[19] which determines the double layer capacitance.[27] A 10 mM sodium phosphate buffer was used to fix the pH at 7.0 ± 0.1 at each of the five concentrations of NaCl: 100, 50, 20, 10, 0 mM. Bulk conductivities of these solutions were interpolated from published values.[44]

(21) Wu, M.-Y.; Smeets, R. M. M.; Zandbergen, M.; Ziese, U.; Krapf, D.; Batson, P. E.; Dekker, N. H.; Dekker, C.; Zandbergen, H. W. *Nano Lett.* **2009**, *9*, 479–484.
(22) Storm, A. J.; Chen, J. H.; Ling, X. S.; Zandbergen, H. W.; Dekker, C. *Nat. Mater.* **2003**, *2*, 537–540.
(23) Fologea, D.; Uplinger, J.; Thomas, B.; McNabb, D. S.; Li, J. *Nano Lett.* **2005**, *5*, 1734–1737.
(24) Karnik, R.; Fan, R.; Yue, M.; Li, D.; Yang, P.; Majumdar, A. *Nano Lett.* **2005**, *5*, 943–948.
(25) Schoch, R.; Han, J.; Renaud, P. *Rev. Mod. Phys.* **2008**, *80*, 839–883.
(26) Stein, D.; Kruithof, M.; Dekker, C. *Phys. Rev. Lett.* **2004**, *93*, 035901/1–035901/4.
(27) Bard, A. J.; Faulkner, L. R. *Electrochemical Methods: Fundamentals and Applications*; John Wiley & Sons: Hoboken, New Jersey, 1980.
(28) Barsoukov, E.; MacDonald, R. *Impedance Spectroscopy: Theory, Experiment, and Applications*, 2nd ed.; John Wiley & Sons: Hoboken, New Jersey, 2005.
(29) Macdonald, J. R. *Impedance Spectroscopy: Emphasizing Solid Materials and Systems*; John Wiley and Sons: Hoboken, New Jersey, 1987.
(30) Ervin, E. N.; White, H. S.; Baker, L. A.; Martin, C. R. *Anal. Chem.* **2006**, *78*, 6535–6541.
(31) Ervin, E. N.; White, H. S.; Baker, L. A. *Anal. Chem.* **2005**, *77*, 5564–5569.
(32) Chilcott, T. C.; Chan, M.; Gaedt, L.; Nantawisarakul, T.; Fane, A. G.; Coster, H. G. L. *J. Membr. Sci.* **2002**, *195*, 153–167.
(33) Macdonald, D. D. *Electrochim. Acta* **2006**, *51*, 1376–1388.
(34) Macdonald, J. R. *Electrochim. Acta* **1990**, *35*, 1483–92.
(35) Kavanagh, J. M.; Hussain, S.; Chilcott, T. C.; Coster, H. G. L. *Desalination* **2009**, *236*, 187–193.
(36) Coster, H.; Chilcott, T. *Surface Chemistry and Electrochemistry of Membranes*; Marcel Dekker, Inc.: New York, 1999.
(37) Coster, H. G. L.; Kim, K. J.; Dahlan, K.; Smith, J. R.; Fell, C. J. D. *J. Membr. Sci.* **1992**, *66*, 19–26.
(38) Gaedt, L.; Chilcott, T. C.; Chan, M.; Nantawisarakul, T.; Fane, A. G.; Coster, H. G. L. *J. Membr. Sci.* **2002**, *195*, 169–180.
(39) Kaiser, H.; Beccu, K. D.; Gutjahr, M. A. *Electrochim. Acta* **1976**, *21*, 539.
(40) Duffy, D. C.; McDonald, J. C.; Schueller, O. J. A.; Whitesides, G. M. *Anal. Chem.* **1998**, *70*, 4974–4984.
(41) McDonald, J. C.; Whitesides, G. M. *Acc. Chem. Res.* **2002**, *35*, 491–499.
(42) Hillborg, H.; Ankner, J. F.; Gedde, U. W.; Smith, G. D.; Yasuda, H. K.; Wikstrom, K. *Polymer* **2000**, *41*, 6851–6863.
(43) Kern, W.; Puotinen, D. A. *RCA Rev.* **1970**, *31*, 187–206.
(44) Weast, C. R., Ed. *CRC Handbook of Chemistry and Physics*; CRC Press, Inc.: Boca Raton, FL, 1989−1990.

These values matched well with conductivity measurements made based on determining the cell constant and instrument without a membrane present but showed some deviations at high ionic strengths. (See the Supporting Information.)

A Gamry Instruments Reference 600 potentiostat was used to apply the potentials and measure the impedance in the system in a standard four-electrode permeation cell mode. In this work, the applied potentials were kept low (10 mV ac amplitude and no dc bias) to minimize any Faradaic reactions. Furthermore, the reference electrodes are connected to a high impedance input and draw negligible current. A total of 67 frequencies were measured ranging from 0.1 Hz to 1 MHz. Measurements were made for each solution condition with and without the membrane present to determine the cell constant and instrument response. Each experiment was repeated four times with a maximum variability of 0.8%, in the magnitude of impedance, and the data reported is the average of these measurements.

Each EIS measurement was subjected to Kramers−Kronig validation using a grid of 300 $R||C$ functions with log-spaced time constants ranging from 9 ns to 400 s to fit using the active set approach.[45] Increasing the resolution and range of the grid did not improve the fits. The residuals were well-behaved with magnitudes that matched the empirically observed run-to-run variability in the data. The equivalent circuit models were implemented in Mathematica 7.0.1 (Wolfram Research), and the data sets were fit using the built in NonlinearModelFit function. The variance of the residuals from the active set fit was used to estimate the per-point variance of the data sets and also used to determine a reduced chi-squared statistic, χ_{red}^2, to evaluate the quality of nonlinear fits to the different equivalent circuit models:

$$\chi_{red}^2 = \frac{\nu_{as}}{\nu_m}\frac{\chi_m^2}{\chi_{as}^2} \tag{1}$$

Here, χ_m^2 and χ_{as}^2 are the summed squared residuals from the equivalent circuit model fit and the active set fit, respectively. The corresponding degrees of freedom are ν_m and ν_{as}. Each of the 67 frequencies used produces an impedance with a real part and an imaginary part; thus, $n = 134$ measurements are made. For the active set fits, $\nu_{as} = n - p$ where p is the number of active elements in the active set fit. For the nonlinear model fits, $\nu_m = n - p$ where p is the number of free fit parameters in the model. Errors in nonlinear model fit parameters were taken from the estimates provided by the NonlinearModelFit function.

RESULTS AND DISCUSSION

Theoretical Model. To account for the possibility of a variable nanocapillary radius a differential equivalent circuit model is invoked as illustrated in Figure 1. (An appendix with a summary of mathematical symbols used is included at the end of the paper.) The approach is similar to that used to construct mathematical models for transmission lines[39,46,47] but with boundary conditions appropriate for the nanocapillary. A differential element of the capillary resistance, $\Delta R(x)$, is added in series with a parallel circuit

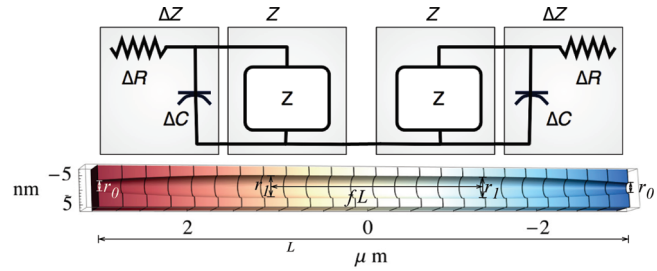

Figure 1. Bottom panel shows a schematic of the nanocapillary geometry with length L, center radius r_1, opening radius, r_0, and a nontapered center fraction f. The variable radius and double layer capacitance of the nanocapillary is accounted for by a differential equivalent circuit shown in the top panel. The two sides are symmetric in the model. The differential equation arising from this circuit and its symmeterized solutions are discussed in the text.

of a differential element of the nanocapillary double layer capacitance, $\Delta C(x)$, and the overall impedance of the capillary, $Z(x)$:

$$Z(x) + \Delta Z(x) = R'(x)\Delta x + \frac{1}{\frac{1}{Z(x)} + i\omega C'(x)\Delta x} \tag{2}$$

Here $i = (-1)^{1/2}$, ω is the angular frequency of the ac signal, and x is the coordinate along the length of the nanocapillary. Expanding the right side in a Taylor series in Δx, dividing by Δx, and evaluating the limit $\Delta x \to 0$ gives the differential equation

$$Z'(x) + i\omega C'(x)Z(x)^2 - R'(x) = 0 \tag{3}$$

where

$$\frac{dR}{dx} = R'(x) = \frac{1}{\pi r^2(x)\kappa_c}, \quad \text{and} \quad \frac{dC}{dx} = C'(x) = 2\pi r(x)\tilde{C} \tag{4}$$

κ_c is the specific conductivity of the solution within the capillary, and $\tilde{C}_c$ is the capillary double layer differential capacitance. In this formulation, a capillary of length zero should have zero impedance and provides the boundary condition, $Z(0) = 0$. The symmetrized circuit element is obtained by solving the differential equation with $r(x)$ proceeding from $x = 0$ to $x = L/2$ and then replacing $r(x)$ by $r(L/2 - x)$ and proceeding again from $x = 0$ to $x = L/2$, to obtain the impedance for the total length, L, for the capillary. To facilitate fitting to the experimental data, closed-form expressions were obtained for three cases of $r(x)$: constant, linear, and quadratic. The resulting functions can be combined to model essentially arbitrary capillary geometries.

Solution for Constant Radius. For a constant radius, $r(x) = r_1$, the solution to eq 3 is

$$Z_{cyl}(\omega) = R_{cyl}\frac{\tanh(\sqrt{i\tau_{cyl}\omega/4})}{\sqrt{i\tau_{cyl}\omega/4}} \tag{5}$$

(45) Giurleo, J. T.; Talaga, D. S. *J. Chem. Phys.* **2008**, *128*, 114114/1–114114/18.
(46) Franceschetti, D. R. *J. Chem. Phys.* **1987**, *86*, 6495–6501.
(47) Chien, M.-C.; Wang, G.-J.; Yu, W.-C. *Jpn. J. Appl. Phys., Part 1* **2007**, *46*, 7436–7440.

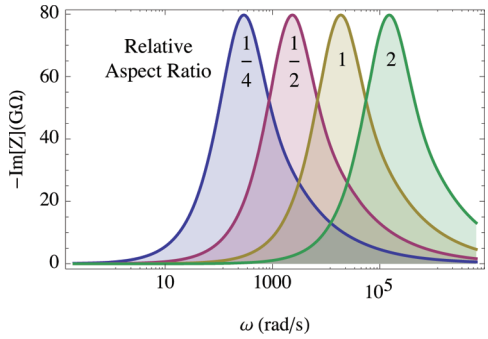

Figure 2. Negative imaginary component of the EIS spectrum gives different peak frequencies depending on the nanocapillary cylindrical aspect ratio r/L. Plots of eq 5 for the same values of R_{cyl} but different aspect ratios are shown. The aspect ratios labeled in the figure are relative to the reference geometry of $L = 6$ μm, $r = 5$ nm with $\kappa_c = 0.4$ S/m, $\tilde{C}_c = 1.5$ mF/m^2.

Equation 5 has the same functional form, but different parametrization, as the finite Warburg impedance.[48−50] Equation 5 can be used to fit the geometry of a cylindrical nanocapillary and has two free parameters for fitting: the dc resistance, R_{cyl}, and a time constant, τ_{cyl}. R_{cyl} and τ_{cyl} have different dependencies on nanocapillary geometry, nanocapillary double layer differential capacitance, and solution conductivity given by

$$R_{cyl} = \frac{L}{\pi r_1^2 \kappa_c} \tag{6a}$$

$$\tau_{cyl} = R_{cyl}C_{cyl} = \frac{2L^2\tilde{C}_c}{r_1\kappa_c} \tag{6b}$$

Changes in the aspect ratio of the nanocapillary for a constant R_{cyl} change the peak frequency in the Nyquist plot, which is obtained by maximizing $-\mathrm{Im}[Z_{cyl}(\omega)]$ from eq 5 giving

$$\omega_{peak} \approx 2.54/\tau_{cyl} \tag{7}$$

By altering the aspect ratio, the capillary surface area is changed. As the surface area increases the overall capacitance of the capillary increases, which increases the time constant and consequently decreases the peak frequency, eq 7. The net effect is a rescaling of the dependence of the spectrum on frequency, an effect best visualized in the plot of the imaginary component of the impedance versus frequency as shown in Figure 2. Scale changes of the parametric variable in parametric plots (e.g., a Nyquist plot) appear as points that shift along a common curve. For a given dc impedance, (R_{cyl}), the peak frequency in the imaginary impedance plot tracks changes in total capillary double layer capacitance while the line shape remains constant. Thus, EIS can distinguish the capillaries aspect ratio based on the peak frequency.

Solution for Linearly Varying Radius. Constriction at the nanocapillary opening results in a lozenge shape, and constriction at the center results in an hourglass shape. Both of theses cases can be treated with a linearly varying capillary radius:

$$r(x) = r_0 + 2x(r_1 - r_0)/L \tag{8}$$

where r_0 is the entrance radius and r_1 is the center radius. Integrating eq 3 using eq 8 gives a variation of the Warburg impedance, referred to as the variable topology finite Warburg impedance or $Z_{VTW}(\omega)$ in this paper for arbitrary geometries. The linear case gives a closed form for lozenge shaped pores and capillaries.

$$Z_{loz}(\omega) = \frac{R_{loz}(I_1(\xi_1)K_1(\xi_0) - I_1(\xi_0)K_1(\xi_1))}{\tau_1 - \tau_0} \times \left(\frac{\tau_1}{\xi_0(I_2(\xi_0)K_1(\xi_1) + I_1(\xi_1)K_2(\xi_0))} + \frac{\tau_0}{\xi_1(I_2(\xi_1)K_1(\xi_0) + I_1(\xi_0)K_2(\xi_1))}\right) \tag{9}$$

where I_n is the modified Bessel function of the first kind of order n and K_n is the modified Bessel function of the second kind of order n. Also with

$$R_{loz} = \frac{L}{\kappa_c \pi r_1 r_0} \tag{10}$$

and

$$\xi_0 = \sqrt{i4\tau_0\omega} \qquad \text{and} \qquad \xi_1 = \sqrt{i4\tau_1\omega} \tag{11}$$

where

$$\tau_0 = \frac{L^2\tilde{C}_c r_0}{2\kappa_c(r_1 - r_0)^2} \qquad \text{and} \qquad \tau_1 = \frac{L^2\tilde{C}_c r_1}{2\kappa_c(r_1 - r_0)^2} \tag{12}$$

The ratio of the time constants is equal to the ratio of the entrance radius and center radius.

$$\frac{\tau_1}{\tau_0} = \frac{r_1}{r_0} \tag{13}$$

Complete details on the derivation of eq 9 are presented in the Supporting Information.

Figure 3 shows the predicted effect of constricting the capillary opening on the EIS data. Capillaries with different degrees of constriction can give the same dc impedance and similar peak frequencies. However, the magnitude of the imaginary component of the EIS data is reduced across the peak as the degree of constriction increases. The time response of the differential impedance element is position-dependent because the relative values of the resistance and capacitance change along the length of the capillary. The changing radius introduces dispersion in the characteristic time constants of the circuit. In this representative example, the net effect of introducing new time scales to the response is to suppress the peak of the spectrum in the Nyquist plot. This effect increases with the degree of constriction of the openings or the center.

(48) Warburg, E. *Ann. Phys.* **1899**, *67*, 493–499.
(49) Macdonald, J. R. *J. Chem. Phys.* **1974**, *61*, 3977–3996.
(50) Franceschetti, D. R.; Macdonald, J. R.; Buck, R. P. *J. Electrochem. Soc.* **1991**, *138*, 1368–1371.

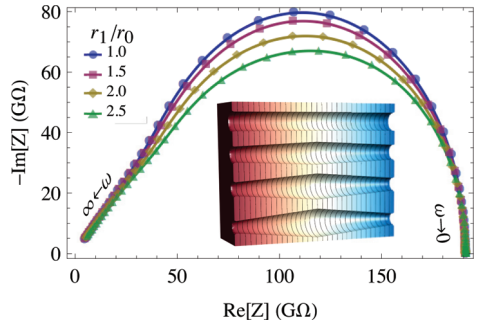

Figure 3. Effect of constriction of the openings of cylindrical nanocapillaries on the EIS spectrum is shown by plotting eq 9 for different ratios of the radii as shown in the figure legend. Each of the four nanocapillaries has the same dc resistance and would in principle give identical current−voltage curves in spite of having vastly different shapes. The EIS shows a clear change with nanocapillary geometry. The parameters used are $L = 6\ \mu$m, $r_1 = 5$ nm, $\kappa_c = 0.4$ S/m, $\tilde{C}_c = 1.5$ mF/m^2. The inset shows renderings of the nanocapillary shapes corresponding to the radii ratios labeled in the figure.

Extension of Z_{VTW} to Other Geometries. Nanopores and nanocapillaries may have many geometries[20] that do not adhere to the simple assumptions of the cylindrical and linear constrictions discussed thus far. The general nature of the variable topology formalism allows determination of an equivalent circuit element for essentially arbitrary geometries by rewriting the differential resistance and capacitance in eq 4. For example, extending the linear Z_{VTW} function to a cone can be accomplished simply by letting L be $2L$ in eq 9, and dividing by 2. To accommodate quadratic changes in capillary radius as a function of length, simply defining $r(x) = r_0 + 4r_1x^2/L^2$ in eq 4 and solving eq 3 leads to a closed form expression for Z_{VTW} involving Legendre functions (see the Supporting Information). Finally, the different Z_{VTW} circuit elements can be combined piecewise to account for different regions of variable nanocapillary radius. For example, the linear circuit element, Z_{loz}, can be combined with cylindrical circuit element, Z_{cyl}, subject to geometric continuity constraints to model a tapered nanocapillary that has a cylindrical center of fractional length f such at that illustrated in Figure 1. The tapered capillary is modeled as the sum of two circuit elements:

$$Z_{VTW} = Z_{cyl} + Z_{loz} \tag{14}$$

the cylindrical center portion of length fL in the center, eq 9, and two tapered regions of total length $(1 - f)L$, eq 5, as illustrated in Figure 1. Thus, in eq 6 L is replaced by fL, and in eqs 10 and 12 L is replaced by $(1 - f)L$. Combining eqs 9 and 5 requires the constraint that the cylindrical portion have the same radius as the end of the adjoining tapered region. The time constant for the cylindrical contribution is now determined by the other time constants:

$$\tau_{cyl} = \frac{4R_{cyl}^{\ 2}\tau_1(\tau_0 - \tau_1)^2}{R_{loz}^{\ 2}\tau_0^{\ 2}} \tag{15}$$

This eliminates τ_{cyl} as a fit variable. More complicated geometries can be built up similarly.

NCAM EIS Consistent with Z_{VTW}. Figure 4 shows the EIS data taken on the NCAM at different solution conductivities. The data without blank subtraction (Figure 4A) is dominated by a semielliptical (suppressed semicircular) feature. A small feature accounting for 1−2% of the total impedance appears at low frequency (below 200 Hz). This feature was larger when using a larger dc potential bias. This feature did not contribute to the blank (Figure 4B) suggesting that it is due to the membrane. A larger feature at high frequency, visible as an up-turn in the Nyquist plot, can be removed by subtraction of the blank data set. After blank subtraction (Figure 4C), the high-frequency limit approaches a phase angle of −55° ± 2° for all cases considered.

NCAM EIS Equivalent Circuit Elements. Figure 3 illustrates the response of a single nanocapillary in isolation, while measured EIS data accounts for additional impedances arising from the effects of the membrane and surroundings. The data shows three distinct features attributable to the instrument response (high frequency), the membrane (low frequency), and the nanocapillaries in the membrane (main peak). The response of the instrument and cell, background, were found to be well-modeled by a two-element equivalent circuit:

$$Z_{bk} = R_{bk}||C_{bk} \tag{16}$$

where Z_{bk}, R_{bk}, and C_{bk}, are, respectively, the impedance, resistance, and capacitance of the electrochemical cell and instrument. Membrane surfaces have been observed to give low-frequency dispersive responses in EIS.[51] To prevent this feature from perturbing the fit of the main nanocapillary response we model the low-frequency feature with a simple $(R_{ms}||C_{ms})$ equivalent circuit. This element accounts for less than 2% of the overall circuit impedance.

NCAMs comprise a large number of capillaries running in parallel across a capacitive polymeric membrane. Adding the impedance Z_{VTW} for each of the N capillaries in parallel with the membrane capacitance C_{mem} gives

$$Z_{sys} = \frac{Z_{VTW}}{N}||C_{mem} \tag{17}$$

Therefore, the overall equivalent circuit model becomes

$$Z_{exp} = Z_{sys} + Z_{bk} + (R_{ms}||C_{ms}) \tag{18}$$

NCAM EIS is Consistent with a Lozenge Geometry. In this section, several models for the nanocapillary response are fit to the experimental data. The number of fit parameters, degrees of freedom, and χ^2 appear in Table 1. The nanocapillary response in eq 18 is represented by a single impedance element, Z_{VTW}.

A simple electrolyte conductor through a capacitive membrane gives a $R||C$ circuit response. Treating a nanocapillary as a conducting element requires a single fit parameter in addition to those that account for the membrane and measurement system. The fits to such a model were very poor (see the Supporting Information) giving a value of $\chi_{red}^2 \sim 4500$. This is to be expected given that the blank-subtracted data in Figure 4C shows that the high-frequency region approaches a phase angle of −55° ± 2° as opposed to the −90° phase angle value predicted by the $R||C$ circuit. Similarly, the peak in the Nyquist plot of the data is

(51) Coster, H. G. L. *Biophys. J.* **1973**, *13*, 118–132.

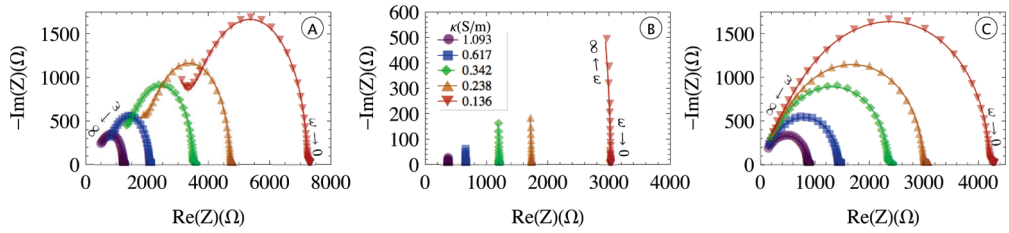

Figure 4. Panel A shows markers for experimental EIS data on a NCAM at five different concentrations of phosphate-buffered NaCl that give conductivities as indicated in the figure legend. Panel B shows the response of the cell and instrument for the same solution conditions. Panel C shows the response of just the membrane obtained by the subtraction of the instrument response from the data. Local fits using eqs 14 and 16 and their difference are shown as solid lines in panels A−C, respectively. Details of the fitting are discussed in the text.

Table 1. Quality of Model Fits

model	$\chi_m^2 \times 10^3$	p	ν	χ_{red}^2
$R\|\|C_{mem}$	7700	30	640	4500
$Z_{cyl}\|\|C_{mem}$	860	35	635	500
$Z_{loz}\|\|C_{mem}$	100	40	630	61
local $(Z_{loz} + Z_{cyl})\|\|C_{mem}$	57	45	625	34
global $(Z_{loz} + Z_{cyl})\|\|C_{mem}$	64	22	658	37
active set	1.5	100	570	1.0

suppressed compared to the $R||C$ circuit. The resistive element is not sensitive to aspect ratio and constrictions. Therefore, the capacitive double layer is a likely candidate for improving the fits since models including it show qualitative features much closer to those of the data as eq 9 predicts and as Figure 3 shows.

Treating the nanocapillaries with the cylindrical model including double layer capacitance, eq 5, requires one additional fit parameter per local fit and improves the fits substantially with χ_{red}^2 reduced by nearly 9-fold. However, the cylindrical model with double layer capacitance still does not capture the degree of suppression of the peak in the Nyquist plot. (See the Supporting Information.)

The presence of constrictions in the nanocapillary is predicted to cause further suppression of the peak in the Nyquist plot as shown in Figure 3. Indeed when the eq 9 is used for the nanocapillary response, all the main features of the data are captured and χ_{red}^2 is reduced further by a factor of 8.2. Nanowires grown in NCAMs have shown that NCAMs may be tapered at the ends.[52−57] Equation 9 implies that the taper is across the entire capillary rather than just at the ends. This geometry can be modeled using eq 14. This further reduces χ_{red}^2 by a factor of 1.8. Since further geometric complexity is difficult to justify based on the present understanding of ion-track etched nanocapillaries, the fits using eq 14 will be the basis for further analysis. The fits to the experimental data using eq 14 are shown as lines in Figure 4. The fit parameters and errors are summarized in Table 2.

Local Fits Reveal Global NCAM EIS Model. There are two types of parameters in the Z_{VTW} impedance element. Geometric parameters such as r_0, r_1, N, and L should be independent of the electrolyte concentration. The capacitance of the double layer should depend on the electrolyte concentration. The changes in EIS with electrolyte concentration allows separation of these effects through a global analysis. Figure 5 shows plots of combinations of the local parameters that allow extraction of the global dependence of the geometric and capacitive properties of the nanocapillaries.

Figrure 5A shows a plot of the combination of parameters that isolates the effective capillary conductivity

$$\kappa_c = \frac{(\tau_0 + \tau_1)^2}{\tau_1(R_{loz}\tau_0 + R_{cyl}\tau_1)} \frac{L}{\pi(r_0 + r_1)^2 N} \tag{19}$$

versus the bulk solution conductivity. The conductivity in the capillary is observed to be linearly related to the bulk conductivity ($\kappa_c = \kappa_b + \kappa_0$) with ($\kappa_0 = 0.105 \pm 0.003$ S/m). The slightly higher conductivity inside the nanocapillary is consistent with the requirement of additional charge to neutralize capillary surface charge.[18] This effect is most noticeable for capillaries with diameters comparable to the Debye length at a given electrolyte concentration.[24,26,58−60]

Figure 5B shows a plot of the ratio of time constants which is related to the ratio of the entrance and center radii through eq 13. The plot shows that the ratio of radii parameter has an average value of 2.0 ± 0.1. Figure 5C shows a plot of the combination of local fit parameters that give the fraction of the nanocapillary length that is cylindrical:

$$f = \frac{\tau_1 R_{cyl}}{\tau_1 R_{cyl} + \tau_0 R_{loz}} \tag{20}$$

Figure 5C shows that the cylindrical fraction parameter has an average value of 0.416 ± 0.009. Both of the geometric nanocapillary parameters show a modest dependence of their values on the conductivity. In both cases the conductivity dependence is smaller than the error in the parameters as propagated from the fit parameters. This small effect is likely due to the covariance of fit parameters in the local nonlinear fitting function.

(52) Schonenberger, C.; Van Der Zande, B. M. I.; Fokkink, L. G. J. *Mater. Res. Soc. Symp. Proc.* **1997**, *451*, 359–365.
(53) Riveros, G.; Gomez, H.; Schrebler, R.; Marotti, R. E.; Dalchiele, E. A. *Electrochem. Solid-State Lett.* **2008**, *11*, K19–K23.
(54) Motoyama, M.; Fukunaka, Y.; Sakka, T.; Ogata, Y. H.; Kikuchi, S. *Proc.—Electrochem. Soc.* **2006**, *2004−19*, 99–108.
(55) De Leo, M.; Pereira, F. C.; Moretto, L. M.; Scopece, P.; Polizzi, S.; Ugo, P. *Chem. Mater.* **2007**, *19*, 5955–5964.
(56) Leopold, S.; Schuchert, I. U.; Lu, J.; Toimil Molares, M. E.; Herranen, M.; Carlsson, J.-O. *Electrochim. Acta* **2002**, *47*, 4393–4397.
(57) Ferain, E.; Legras, R. *Nucl. Instrum. Methods Phys. Res., Sect. B* **2001**, *174*, 116–122.
(58) Desgranges, C.; Delhommelle, J. *Phys. Rev. E: Stat., Nonlinear, Soft Matter Phys.* **2008**, *77*, 027701/1–027701/4.
(59) Schoch, R. B.; van Lintel, H.; Renaud, P. *Phys. Fluids* **2005**, *17*, 100604/1–100604/5.
(60) Tang, Y. W.; Szalai, I.; Chan, K.-Y. *Mol. Phys.* **2001**, *99*, 309–314.

Table 2. Parameters for Local Fits to $Z_{VTW} = Z_{cyl} + Z_{loz}$

NaCl mM	buffer mM	κ_b S/m	τ_0 μs	τ_1 μs	R_{cyl}/N Ω	R_{loz}/N Ω
100	10	1.093 ± 0.004	1.6 ± 0.8	4.0 ± 1.3	226 ± 4	644 ± 11
50	10	0.617 ± 0.002	3.9 ± 1.0	8.8 ± 1.6	360 ± 6	1070 ± 14
20	10	0.342 ± 0.001	8.2 ± 1.9	17 ± 3	598 ± 9	1740 ± 20
10	10	0.238 ± 0.001	14 ± 3.5	27 ± 5	788 ± 13	2198 ± 24
0	10	0.136 ± 0.001	31 ± 7.6	52 ± 10	1180 ± 20	3024 ± 30

Figure 5D shows a plot of the combination of parameters that isolates the differential capacitance of the nanocapillary interior:

$$\tilde{C}_c = \frac{2(\tau_0 - \tau_1)^2(\tau_1 R_{cyl} + \tau_0 R_{loz})}{\pi r_1 \tau_0^2 R_{loz}^2 LN} \qquad (21)$$

The differential capacitance showed a square root dependence on solution conductivity ($\tilde{C}_c = \tilde{C}_0 + \tilde{C}_1(\kappa_b)^{1/2}$) with $\tilde{C}_0 = 1.12 \pm 0.03$ mF/m^2 and $\tilde{C}_1 = 0.53 \pm 0.04$ mF/m^2 (m/S)$^{1/2}$. The square root power law is consistent with a simple Gouy−Chapman interpretation of the double layer capacitance.[61−63]

EIS Global Fitting Gives NCAM Geometry. To obtain final nanocapillary geometric properties, the data was subjected to a global fit to eq 14. The dependencies of the local fit parameters on the nanocapillary properties are defined by eqs 12, 9, 6a, and 6b with the total length parameter replaced by the appropriate fractional length as discussed for eq 14. The global analysis directly fit the nanocapillary geometric properties r_0, r_1, f as independent of bulk conductivity. The parameters that control the bulk conductivity dependence of differential capacitance and the capillary conductivity ($\tilde{C}_0$, $\tilde{C}_1$, and κ_0) are also reoptimized by the global fit. The background circuit element was globally modeled as a simple electrolyte solution resistor ($R_{bk} = R_{cell}/\kappa_b$) with a power-law conductivity-dependent capacitance constant ($C_{bk} = C_{1bk}\kappa_b^{3/2} + C_{0bk}$). The same power law functions were observed to fit the instrument response of both the background measurement and the NCAM measurement. The cell constant, R_{cell}, was the also the same within experimental uncertainty. (See the Supporting Information.) The low-frequency circuit element (10 parameters) was not reoptimized from the local values that appear in the Supporting Information. The parameters L, N, and C_{mem} were allowed to float after initial convergence.

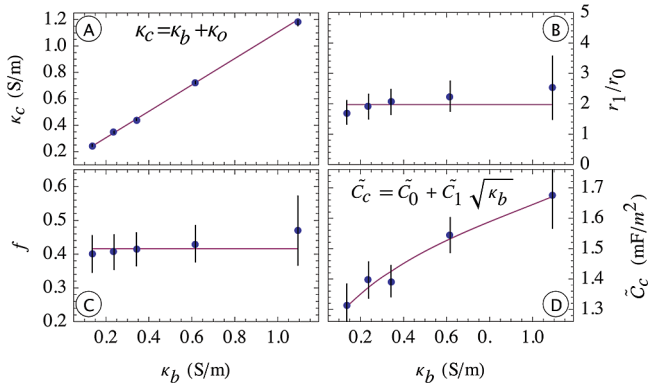

Figure 5. Local fit parameters were plotted in combination (points) to obtain the global dependence (fit lines) of nanocapillary parameters as discussed in the text. Error bars were propagated from the standard errors from the fit parameters. Panel A shows the capillary conductivity vs the bulk conductivity. A linear dependence is found with a constant offset to account for surface charge counterions in the nanocapillary. Panel B shows the ratio of the radii, r_1/r_0. Panel C shows the fraction, f, of the length, L, of the capillary that is cylindrical. Panel D shows the capillary double layer differential capacitance and a fit to a square-root power law.

Table 3. NCAM EIS Global Fit Parameters

r_0	2.19 ± 0.01 nm
r_1	4.05 ± 0.01 nm
f	0.408 ± 0.007
κ_0	0.109 ± 0.001 S/m
$\tilde{C}_0$	1.21 ± 0.05 mF/m^2
$\tilde{C}_1$	0.36 ± 0.09 mF/m^2(m/S)$^{1/2}$
R_{cell}	410 ± 2 m^{-1}
C_{0bk}	7.8 ± 1.8 pF
C_{1bk}	58 ± 26 pF(m/S)$^{3/2}$
N	1.70 ± 0.01 × 10^8
L	6.00 ± 0.03 μm
C_{mem}	139 ± 17 pF

Table 3 shows the 12 global fit parameters. The uncertainties in Table 3 were estimated based on the diagonal elements of the covariance matrix of the χ^2 surface for the global fit. For many of the parameters these estimates appear to be unrealistically small if interpreted as uncertainties in the determination of the parameter. Use of the covariance matrix to determine parameter uncertainties is based on the assumption that all variance is due to random errors. The magnitude of the active set fit residuals was consistent with random noise in the measurement. The squared residuals for both the local and global fits are a factor of ~ 35 larger than those of the active set implying that there is some aspect of the NCAM response not being accounted for in the model vida infra. In this case the uncertainties in the parameters as determined from the diagonal covariance matrix elements must be interpreted as measures of how well the parameter is defined by the fitting procedure.

Possible Model Limitations. The equivalent circuit model fits the data well and is able to produce a quantitative estimate of the nanocapillary geometry. However, the fit residuals result in a value of χ_{red}^2 that suggest that the model is still incomplete. There are several aspects of the equivalent circuit model where improvement in the physical description of the model could lead to a better fit to the data. Since any of the improvements could be invoked, none should be without specific evidence. In each case there is no evidence compelling the increase in complexity. Therefore inclusion of these phenomena is beyond the scope of the present work.

(61) Kornyshev, A. A. *J. Phys. Chem. B* **2007**, *111*, 5545–5557.
(62) Bockris, J. O.; Reddy, A. K.; Gamboa-Aldeco, M. E. *Modern Electrochemistry 2A: Fundamentals of Electrodics*, 2nd ed.; Plenum Publishing Corporation: New York, 2001.
(63) Eijkel, J. C. T.; van den Berg, A. *Chem. Soc. Rev.* **2010**, *39*, 957–973.

Though the Z_{VTW} approach can accommodate a distribution of nanocapillary radii and/or shape, the current model does not include any contribution from nanocapillary geometric heterogeneity; it assumes all nanocapillaries have the same geometry. Adding a distribution of geometries would increase the dispersion of the time scales in the main EIS feature and would lead to an improvement in the fit. However, ion-track etched nanocapillaries are reported to be largely homogeneous in geometry.[52,54,56] Attributing the dispersion of the nanocapillary contribution to the EIS signal would imply a distribution of capillary cylindrical radii covering a range of ~2.5 times the average radius. This is in significant excess of the specified and observed distribution of ion-track etched nanocapillaries.

The range of time constants present in the component attributed to the membrane could include contributions outside of the low-frequency region that the equivalent circuit model currently treats. The phenomenological treatment of these low-frequency contributions is descriptive and invokes serial $R||C$ circuits. To resolve any possible overlap between these dispersive membrane contributions to the EIS and the nanocapillary response would require a better phenomenological description than serial $R||C$ circuits. Until such treatments are available this sort of ambiguity is likely to persist.

The geometry used to solve Z_{VTW} and treat the nanocapillaries may be too simplistic to represent the real nanocapillaries. The present model exhibiting tapered ends with an approximately cylindrical center is most complicated overall geometry that has been confirmed to be present in NCAMs.[52−57] Independent characterization of any variability of the nanocapillary radius is needed to provide justification for additional geometric complexity.

The surface of the polycarbonate membrane is coated with poly(vinylpyrrolidone). This detail is not distinguished in the model. Given the thinness of the PVP passivation layer, it is unlikely that it would contribute significantly to the impedance of the circuit.

The double layer differential capacitance is treated as a simple differential capacitor element.[27] The actual response of the double layer is likely more complicated. It has been proposed to use multiple $R||C$ components in order to separate the electrical double layer into the more diffuse Gouy−Chapman layer and inner, more compact Stern layer.[38] Substitution of a more complicated model for the differential capacitor element would increase the dispersion of Z_{VTW} and possibly improve the fit. However, as with the other examples of added model complexity, there is no independent evidence to prefer this approach to improving the fit over the others already discussed.

Comparison of Fit Parameters and Manufacturer's Specifications. The fit parameters suggest that the openings to the nanocapillaries are constricted by a factor of 1.85 from their centers. Several imaging studies have shown that the nanocapillaries are wider the middle as compared to the entrance and exit.[52−57] The middle region of nanocapillaries can be wider than the entrance and exit by almost 3 times in some cases.[52]

The fit parameters indicate a nanocapillary entrance (and exit) radius of 2.19 ± 0.01 nm and a center radius of 4.05 ± 0.01 nm. The manufacturer reports the nominal radius to be 5 nm, with a tolerance between 0 and −20% (or 4.5 ± 0.5 nm), a membrane thickness of 6 μm with a tolerance of ±10%, and a capillary density of 6×10^8 capillaries/cm^2 with a tolerance of ±15%. Therefore, the fit parameter for the center radius is at the low end of the manufacturer's specifications. The uncertainty in the membrane thickness and nanocapillary number density together could change the estimated opening and center radii to be 2.49 and 4.61 nm, respectively. Several additional phenomena could account for a systematic underestimation of the nanocapillary radii.

The mobility of ions in the electrical double layer is expected to be reduced compared to those in the bulk. Such effects of electroviscosity[25,64] are not explicitly incorporated into the model. It is possible that such an effect would increase the impedance of the nanocapillary. The net effect in fitting the present model would be to underestimate the nanocapillary radii to compensate for the added impedance. An improvement to the present model might, therefore, be to add a differential resistive element in series with the double layer differential capacitive element. The low-frequency component that was attributed to the membrane surface was modeled as a single $R||C$ circuit. The active set fits indicated that this component was very dispersive in nature requiring six $R||C$ components covering at least 4 decades in decay time. It is possible that the membrane surface response also included impedance in the same spectral region as the nanocapillaries. In this case the additional impedance would manifest as a smaller nanocapillary radius in the fitting.

Both the membrane thickness and capillary number density are coupled in the fitting to the capillary geometry. If the thickness of the membrane during the experiment is larger than that specified or if the number density of the nanocapillaries is lower than that specified, then the nanocapillaries radius will be underestimated. Changing membrane thickness will also influence the membrane capacitance. However, for changes in C_{mem} consistent with the variability of the membrane thickness, essentially no changes were observed for the geometric parameters.

CONCLUSION

An analytical modeling approach for extracting nanocapillary geometry and double layer differential capacitance from EIS data has been presented and validated experimentally through measurement on a commercial NCAM. By exploiting the differences between the nanoscale and the bulk response to changes in electrolyte concentration, the model provides a quantitative estimate for the nanocapillary geometry. The methodology presented in this work is expected to be of interest to the larger community of nanopore and nanocapillary investigators due to the noninvasive nature of the technique.

ACKNOWLEDGMENT

This project was supported in part by award no. R01GM071684 from the National Institute of General Medical Sciences. The content is solely the responsibility of the authors and does not necessarily represent the official views of the National Institute of General Medical Sciences or the National Institutes of Health. The authors thank the National Science Foundation for partial support of this work through Grant CBET 0813944. The authors

(64) Tas, N. R.; Haneveld, J.; Jansen, H. V.; Elwenspoek, M.; van den Berg, A. *Appl. Phys. Lett.* **2004**, *85*, 3274–3276.

thank Steve Dulin at GE Osmonics for valuable discussions of the NCAM properties.

Nomenclature List

Z	impedance [Ω]
R	resistance [Ω]
R'	dR/dx [Ω/m]
C'	dC/dx [F/m]
ω	angular frequency [rad/s]
i	$(-1)^{1/2}$ [ ]
r	radius [m]
$\tilde{C}_c$	capillary double layer differential capacitance [F/m^2]
κ_c	capillary conductivity [S/m]
κ_b	bulk conductivity [S/m]
L	capillary length [m]
Z_{cyl}	cylindrical impedance model [Ω]
Z_{loz}	lozenge impedance model [Ω]
Z_{VTW}	variable topology finite Warburg impedance [Ω]
R_{cyl}	resistance of a cylinder [Ω]
R_{loz}	resistance of a lozenge [Ω]
r_0	entrance (and exit) radius [m]
r_1	center radius [m]
f	fraction cylindrical length of nanocapillary [ ]
τ_{cyl}	time constant for constant radius capillary [s]
τ_0	time constant for r_0 in Z_{loz} [s]
τ_1	time constant for r_1 in Z_{loz} [s]
C_{mem}	membrane capacitance [F]
N	number of capillaries [ ]
A_{mem}	membrane area [m^2]
R_{ms}	resistance of external membrane surface [Ω]
C_{ms}	capacitance of external membrane surface [F]
R_{bk}	cell and instrument resistance [Ω]
R_{cell}	cell constant [m^{-1}]
C_{bk}	cell and instrument capacitance [F]
C_{0bk}	constant coefficient in C_{bk} fit [F]
C_{1bk}	$\kappa^{3/2}$ coefficient in C_{bk} fit [F (m/S)$^{3/2}$]
Z_{bk}	cell and instrument impedance [Ω]
Z_{exp}	experiment impedance [Ω]
Z_{sys}	system impedance [Ω]
κ_0	increased capillary conductivity offset [S/m]
$\tilde{C}_0$	constant coefficient in $\tilde{C}_c$ fit [F/m^2]
$\tilde{C}_1$	square root coefficient in $\tilde{C}_c$ fit [F/m^2(m/S)$^{1/2}$]
ν	degrees of freedom [ ]
p	number of fit parameters [ ]
χ_m^2	chi-squared model [Ω^2]
χ_{as}^2	chi-squared active set [Ω^2]
χ_{red}^2	reduced chi squared [ ]

SUPPORTING INFORMATION AVAILABLE

A derivation of the Z_{VTW} circuit element for cylindrical, lozenge, conical, and quadratic geometries; the results of the active set fitting; the global fitting of the instrument response; the calibration of the bulk conductivity and cell constant; the local fits to the experimental data using $R||C_{mem}$, $Z_{cyl}||C_{mem}$, and $Z_{loz}||C_{mem}$; the parameters for the membrane surface and instrument response for the local fits to eq 14; the global fits of the data to eq 14; a schematic of the experimental setup. This material is available free of charge via the Internet at http://pubs.acs.org.

Received for review August 25, 2010. Accepted November 15, 2010.

AC102236K